Title

Effects of Stellar Feedback on Stellar and Gas Kinematics of Star-forming Galaxies at 0.6 < z < 1.0

Journal

Astrophysical Journal Letters, 896(2)

ISSN

2041-8205

Authors

Pelliccia, D
Mobasher, B
Darvish, B
et al.

Publication Date

2020-06-20

DOI

10.3847/2041-8213/ab9815

Peer reviewed

Draft version January 6, 2020
Typeset using LaTeX **twocolumn** style in AASTeX63

Effects of Stellar Feedback on Stellar and Gas Kinematics of Star-Forming Galaxies at $0.6 < z < 1.0$

Debora Pelliccia,[1,2] Bahram Mobasher,[1] Behnam Darvish,[3] Brian C. Lemaux,[2] Lori M. Lubin,[2] Jessie Hirtenstein,[2] Lu Shen,[4] Po-Feng Wu,[5] Kareem El-Badry,[6] Andrew Wetzel,[2] and Tucker Jones[2]

[1]*Department of Physics and Astronomy, University of California, Riverside, 900 University Ave, Riverside, CA 92521, USA*
[2]*Department of Physics, University of California, Davis, One Shields Ave, Davis, CA 95616, USA*
[3]*Cahill Center for Astrophysics, California Institute of Technology, 1216 East California Boulevard, Pasadena, CA 91125, USA*
[4]*CAS Key Laboratory for Research in Galaxies and Cosmology, Department of Astronomy, University of Science and Technology of China, Hefei 230026, China*
[5]*National Astronomical Observatory of Japan, Osawa 2-21-1, Mitaka, Tokyo 181-8588, Japan*
[6]*Department of Astronomy and Theoretical Astrophysics Center, University of California Berkeley, Berkeley, CA 94720*

(Received; Revised; Accepted)

Submitted to ApJL

ABSTRACT

Recent zoom-in cosmological simulations have shown that stellar feedback can flatten the inner density profile of the dark matter halo in low-mass galaxies. A correlation between the stellar/gas velocity dispersion (σ_{star}, σ_{gas}) and the specific star formation rate (sSFR) is predicted as an observational test of the role of stellar feedback in re-shaping the dark matter density profile. In this work we test the validity of this prediction by studying a sample of star-forming galaxies at $0.6 < z < 1.0$ from the LEGA-C survey, which provides high signal-to-noise measurements of stellar and gas kinematics. We find that a correlation between σ_{star} (and σ_{gas}) and sSFR indeed exists for galaxies in the lowest mass bin ($M_* \sim 10^{10}\,M_\odot$). This correlation holds for different tracers of star formation, and becomes stronger with redshift. This result generally agrees with the picture that at higher redshifts star formation rate was generally higher, and galaxies at $M_* \lesssim 10^{10}\,M_\odot$ have not yet settled into a disk. As a consequence, they have shallower gravitational potentials more easily perturbed by stellar feedback. The observed correlation between σ_{star} (and σ_{gas}) and sSFR supports the scenario predicted by cosmological simulations, in which feedback-driven outflows cause fluctuations in the gravitation potential which flatten the density profiles of low-mass galaxies.

Keywords: galaxies: evolution – galaxies: kinematics and dynamics – techniques: spectroscopic – techniques: photometric

1. INTRODUCTION

Understanding galaxy formation in the context of the cosmological framework is still an open question in astrophysics. While the Λ cold dark matter (ΛCDM) cosmological model successfully explains structure formation in the universe (e.g., Spergel et al. 2007; Komatsu et al. 2011), dark matter only simulations have raised problems for this model, especially on small scales. These N-body simulations predict steep (or 'cuspy') dark matter inner density profiles (e.g., Navarro, Frenk, & White 1997); however, observations have shown that the dark matter profiles of low-mass galaxies can be shallower than the predictions (e.g., Spano et al. 2008; Oh et al. 2011).

E-mail: dpelliccia@ucdavis.edu

Recent works showed that adding a baryonic component to cosmological simulations can resolve the disagreements between predictions and observations for low-mass galaxies ($M_* \leq 10^{9.5}\,M_\odot$, see e.g., Navarro et al. 1996; Read & Gilmore 2005; Pontzen & Governato 2012; Governato et al. 2012; Chan et al. 2015). Stellar feedback may be able to alter the dark matter distribution of dwarf galaxies through bursts of star formation and subsequent gas outflows, which displace enough mass to significantly flatten the central dark matter profile. Low-mass galaxies have shallow gravitational potentials, and therefore are especially sensitive to stellar feedback.

El-Badry et al. (2016, 2017), using the Feedback In Realistic Environments (FIRE; Hopkins et al. 2014) simulations, showed that feedback-driven potential fluctuations cause strong fluctuations in stellar kinematics of low-mass galaxies ($M_* \leq 10^{9.5}\,M_\odot$). Moreover, they found that galaxy specific star formation rate (sSFR) and line-of-sight stellar velocity dispersion (σ_{stars}) have similar time-evolution, e.g., σ_{stars} is higher during episodes of higher sSFR (although with an offset of $\sim$50 Myr). El-Badry et al. (2016) showed a similar trend also for the gas velocity dispersion (σ_{gas}). This correlation is interpreted as a consequence of the galaxy gravitational potential (probed by σ_{stars} and σ_{gas}) being deepest when cold gas accumulates in the galactic center, which is also when the sSFR is highest. El-Badry et al. (2017) suggested that the predicted positive correlation between σ_{stars} and sSFR could be used as an observational test to determine whether real galaxies undergo feedback-driven potential fluctuations as shown in the simulations, and therefore, whether stellar feedback is able to regulate galaxy stellar and dark-matter densities.

This prediction was observationally supported by Cicone et al. (2016) for a large sample of isolated galaxies with $M_* \lesssim 10^{10}\,M_\odot$ in the local universe, and by Hirtenstein et al. (2019) for a sample of gravitationally lensed low-mass galaxies ($M_* = 10^8 - 10^{9.8}\,M_\odot$) at $z \sim 2$ using gas kinematics to trace the galaxy potential. Observational evidence of the effect of stellar feedback on stellar kinematics is still missing beyond the local universe. At higher redshifts, galaxies have typically higher gas fractions at fixed stellar mass (as much as five times, see e.g., Schinnerer et al. 2016), and experience stronger episodes of star formation (e.g., Madau & Dickinson 2014), which could displace enough mass to alter the dark matter halo profile even for more massive galaxies. Zoom-in cosmological simulations by Macciò et al. (2012) and Mollitor et al. (2015) have shown that reasonably strong baryonic feedback can also alter the dark matter density profiles of the progenitors of Milky-Way mass galaxies ($M_{tot} \approx 10^{12}\,M_\odot$) at intermediate redshifts. Moreover, Macciò et al. (2012) compared the dark matter density profiles of two Milky Way-like simulated galaxies, one with strong and one with weak stellar feedback, and found that only the one with stronger feedback was able to flatten the density profile. They showed that the flattening starts at intermediate redshifts ($z \approx 1-2$), when strong star formation and the subsequent energy transfer from feedback in shallower gravitational potentials has the strongest effect.

To observationally explore this hypothesis we investigated whether stellar and gas kinematics and sSFR are correlated for a sample of star-forming galaxies at $0.6 < z < 1.0$. This sample was taken from the Large Early Galaxy Astrophysics Census (LEGA-C; van der Wel et al. 2016) survey, which provides high signal-to-noise stellar and gas kinematics measurements. This Letter is organized as follows. In Section 2 we introduce the data and our sample selection. In Section 3 we describe the methods used to derive our sSFR measurements. The core of the analysis is presented in Section 4. We discuss and summarize our results in Section 5.

Throughout this Letter, we adopt a Chabrier (2003) initial mass function and a ΛCDM cosmology with $H_0 = 70$ km s^{-1}, $\Omega_\Lambda = 0.7$, and $\Omega_M = 0.3$.

2. DATA

2.1. *LEGA-C Survey*

The data used in this study are taken from data release 2 (DR2; Straatman et al. 2018) of the LEGA-C survey, which is a spectroscopic campaign carried out with the VIsible Multi-Object Spectrograph (VIMOS; Le Fèvre et al. 2003) on the ESO Very Large Telescope (VLT) aiming to study the stellar kinematics of K_s-band selected galaxies at $0.6 < z < 1.0$ in the COSMOS fields. The K_s-band limit ranges from $K < 21.08$ at $z = 0.6$ to $K < 20.36$ at $z = 1.0$, and results in a stellar mass limit of the order of $\sim 10^{10}\,M_\odot$. We note that in the DR2 catalog, a small fraction ($\sim$20%) of galaxies are fainter than those limits, since they were observed to fill up the VIMOS masks (see van der Wel et al. 2016; Straatman et al. 2018, for more details on the selection process). We did not exclude those galaxies from our selection (described below); therefore, our sample has a small percentage of galaxies with stellar mass down to $\sim 10^9\,M_\odot$. Observations of 20-hour integration have been performed using the high-resolution grism $HR-red$ (R = 2500) to obtain spectra over a wavelength range $\sim$6300 Å–8800 Å, with spectral resolution (FWHM) of $\sim$ 3 Å and typical signal-to-noise (S/N)$\gtrsim$10 Å^{-1} on the continuum, required to extract the stellar kinematics. Examples of LEGA-C spectra are shown in van der Wel et al. (2016) and Straatman et al. (2018).

Measurements of the observed integrated gas and stellar velocity dispersions (σ_{gas}, σ_{stars}) are publicly released in DR2, and performed by using the Penalized Pixel-Fitting (pPXF, Cappellari & Emsellem 2004; Cappellari 2017) code, which fit each 1D spectrum with a combination of high resolution stellar population templates and emission lines, downgraded to match the resolution of the LEGA-C spectra (see Straatman et al. 2018 and Bezanson et al. 2018 for a full description and examples of the pPXF fits). Values of σ_{gas} and σ_{stars} are measured as the widths of the emission and absorption lines, respectively, and represent the integrated velocity along the line of sight. This includes the contribution of both rotational and turbulent motions, tracing the underlying galaxy's total mass distribution (including stellar, gas, and dark matter components).

In addition, when available, LEGA-C DR2 provides measurements of fluxes (obtained by integrating the pPXF best-fit emission lines) and equivalent widths (EWs) for emission lines visible in the VIMOS spectral range (i.e., [O II]λ3727, H$\delta\lambda$4102, H$\gamma\lambda$4341, H$\beta\lambda$4861, [O III]λ4959, [O III]λ5007), as well as spectroscopic red-

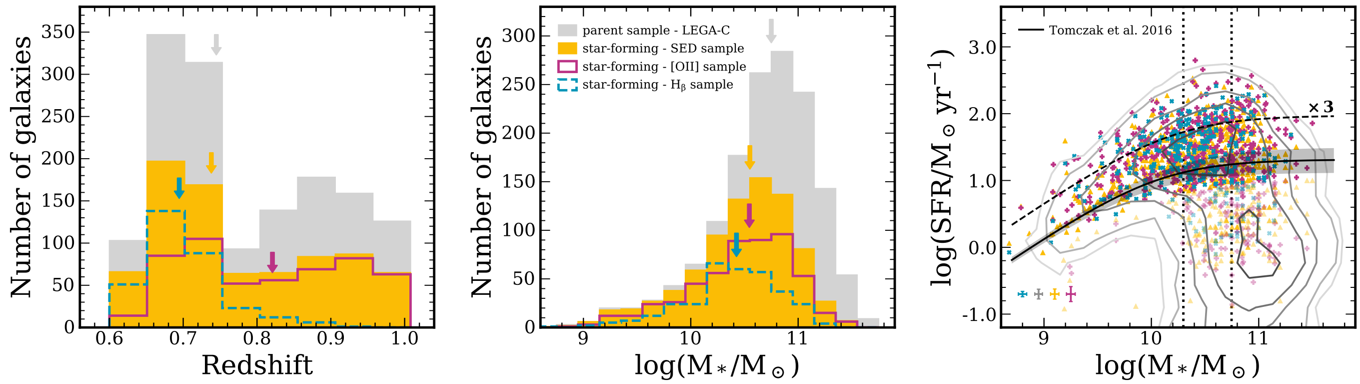

Figure 1. Redshift (left-hand panel) and stellar mass (middle panel) distributions for the parent LEGA-C spectroscopic sample (gray) compared to the distributions for the star-forming SED (yellow), [O II] (magenta), H_{β} (blue) samples (see Section 2). The arrows point to the median value of each distribution. *Right-hand panel:* SFR versus M_*. Values of SFR_{SED} are plotted for the parent LEGA-C (gray contours) and SED (yellow triangles) samples, while $SFR_{[O\,II]}$ and $SFR_{H\beta}$ (Section 3) are plotted for the [O II] (magenta plus signs) and H_{β} (blue crosses) samples, respectively. The median uncertainties in each samples are shown in the bottom-left corner. The contours show the 90%, 70%, 50%, 30% and 10% of the density distribution of the parent sample. The triangles, plus signs and crosses in lighter colors show the galaxies with SFR lower than 0.3 *dex* below the relation (black line) for star-forming only galaxies at $z = 0.8$ from Tomczak et al. (2016) (see discussion in Section 2). The shaded region shows the redshift evolution of SFR-M_* relation between $z = 0.6$ and $z = 1.0$. The black dashed line shows the limit above which galaxies are classified as starbursts (e.g., Elbaz et al. 2018). The black dotted vertical lines show the mass range of the M_* bins used in the analysis in Section 4.

shifts (z_{spec}), Lick/IDS indices (Worthey & Ottaviani 1997), S/N measurements and quality flags (Straatman et al. 2018), which helped us to select a sample of galaxies with only high quality measurements (see Section 2.3).

2.2. *COSMOS2015 Catalog*

Ancillary data are available from the COSMOS2015 photometric catalog (Laigle et al. 2016), which provides accurate spectral energy distribution (SED) fitting measurements, based on deep thirty-band UV–IR photometry that covers all galaxy types. From this catalog we used measurements of stellar mass (M_*), star formation rate (SFR_{SED}), specific SFR ($sSFR_{SED}$), stellar color excess E(B-V)$_*$, and "star-forming/quiescent" classification. The latter, which is based on the NUVrJ color-color diagram (see Laigle et al. 2016, for more detail), was used to select only star-forming galaxies for our investigation of the possible correlation between sSFR and velocity dispersion (see Section 2.3). Although these measurements have been performed by fixing redshifts in the SED fitting to their photometric redshift (z_{phot}) values, we found that, in general, z_{spec} and z_{phot} agree well with a normalized median absolute deviation in $|z_{spec} - z_{phot}|/(1 + z_{spec})$ of 0.008 and with only a few strong outliers: 0.4% with $|z_{spec} - z_{phot}|/(1 + z_{spec}) > 0.1$. We are, therefore, confident that adopting the COSMOS2015 physical parameters at z_{phot} is not degrading our analysis.

2.3. *Sample Selection*

Out of the 1988 galaxies in the LEGA-C public catalog we discarded 368 galaxies for which issues with the quality of the spectrum and/or data reduction were observed, redshift could not be measured, pPXF fit was clearly bad, or had issues with the interpretation of the measurements (see Straatman et al. 2018, for more details on the quality flags). Moreover, we restricted the sample to galaxies in the redshift range of $0.6 < z_{spec} < 1.0$ (galaxies at lower/higher redshifts were observed to fill the VIMOS masks), and removed 47 galaxies that presented spectral duplicates, reducing the sample to 1474 galaxies.

After cross-matching this LEGA-C selected sample with the COSMOS2015 catalog, we found that eight galaxies did not have a match and 69 galaxies are flagged as X-ray sources (see Laigle et al. 2016, for more detail) that suggested a possible AGN contamination. We decided to remove those galaxies, and after selecting only star-forming galaxies following the COSMOS2015 classification (see Section 2.2), the sample was reduced by $\sim 40\%$, leaving us with 815 galaxies.

As we will describe in the next section, we performed our investigation of possible correlation between sSFR and velocity dispersion by adopting three measures of star formation: SED fitting, spectroscopic $H\beta$ and [O II] fluxes. While our full sample (which we call "SED sample") of 815 galaxies have $sSFR_{SED}$ measurements, for 30 of those galaxies σ_{gas} is not available. Moreover, the full sample is further reduced when we consider galaxies with available Hβ and [O II] fluxes at S/N>5, which is a cut that we apply to retain only high-quality flux measurements used for SFR estimates. Therefore, besides the "SED sample", we used in our analysis an "[O II] sample" and "Hβ sample" with 531 and 323 star-forming galaxies, respectively.

The properties of our three sub-samples are shown in Figure 1. In particular, the right-hand plot shows the SFR plotted against M_*, and we can see that at $M_* \lesssim 10^{10}\,M_\odot$ all the three samples and the parent LEGA-C sample lack galaxies with low star formation, i.e., galaxies that are below the SFR–M_* relation typical for normal star-forming galaxies (e.g., Tomczak et al. 2016). This is a consequence of LEGA-C being a magnitude-selected survey, and therefore, the lower mass galaxies that are bright enough to be observed are the ones with higher star formation. Since in our analysis (detailed in Section 4) we investigated the possible correlation between sSFR and velocity dispersion in three different M_* bins (whose boundaries are delineated by the dotted vertical line in Figure 1), we decided to focus only on the *upper* part of the SFR–M_* relation in order to be able to make fair comparisons across all stellar masses. We therefore removed from our sample all galaxies (shown by markers in lighter colors in the plot in Figure 1) with SFR lower than 0.3 *dex* below the SFR–M_* relation for star-forming galaxies at $z = 0.8$ from Tomczak et al. (2016)[1]. The value of 0.3 *dex* was chosen to roughly take into account the redshift evolution of the relation and the average uncertainties on the SFR measurements. This further cut left us with the final "SED sample", "[O II] sample" and "Hβ sample" having 578, 399[2], 267 galaxies, respectively. We note that these three samples have 120 galaxies in common.

3. SPECIFIC STAR FORMATION RATE MEASUREMENTS

In order to investigate the correlation between sSFR and velocity dispersion, we adopted three measurements of sSFR: one that comes from SED fitting (from the COSMOS2015 catalog), which traces a galaxy's star formation integrated over a relatively long period of time (~100 Myr), and two from [O II] and Hβ derived SFR ($SFR_{[O\,II]}$ and $SFR_{H\beta}$, respectively), which are more sensitive to recent star formation episodes (~10 Myr timescale). We applied an internal extinction correction to the emission line fluxes from the LEGA-C catalog, based on the stellar continuum reddening calculated from the SED fitting, and the Calzetti et al. (2000) reddening curve. Following Wuyts et al. (2013), dust attenuation due to the gas ($A_{\rm gas}$) is derived from the SED fitting stellar continuum attenuation ($A_{\rm SED}$) using the relation: $A_{\rm gas} = 1.9\,A_{\rm SED} - 0.15A_{\rm SED}^2$. This dust correction was derived by Wuyts et al. (2013) for a large sample of massive ($M_* > 10^{10}\,M_\odot$) star-forming galaxies at $0.7 < z < 1.5$, and it is widely used in literature (e.g., Stott et al. 2016; Pelliccia et al. 2017; Swinbank et al. 2017). Moreover, it shows a good agreement with the dust attenuation measured from Balmer decrement for stellar masses similar to the ones probed in this study (Price et al. 2014).

We decided not to use higher order Balmer decrement (i.e., Hγ/Hβ or Hδ/Hβ) to estimate dust extinction, since fluxes for Hγ and Hδ emission lines with S/N$>$ 5 are only observationally accessible (in conjunction with Hβ fluxes) for ~25% of our sample of star-forming galaxies. Moreover, obtaining reliable flux measurements for those Balmer lines is challenging, given their intrinsic weakness and the combined effects of stellar absorption and dust extinction (e.g., Moustakas et al. 2006). For the small sample of galaxies for which we could measure the Balmer decrement, we found that ~40% showed Hγ/Hβ and Hδ/Hβ ratios higher than the theoretical values (i.e., 0.47 and 0.26, respectively, Osterbrock & Ferland 2006) and the majority of the remaining galaxies showed inconsistent extinction values measured from two Balmer ratios (in general lower extinction values from Hδ/Hβ). An over correction for stellar absorption of Hγ and Hδ fluxes could explain the observed behavior, considering the weakness of those lines (EW(Hγ) ~ -3.3Å and EW(Hδ) ~ -1.7Å on average) and the strength of the measured stellar absorption (Lick/IDS indices H$\gamma_A \sim 4$Å and H$\delta_A \sim 5.6$Å on average). Hβ flux could also be affected by the over correction of stellar absorption, but since it is a stronger line (median EW(Hβ)~ -6Å), we would expect the effect to be negligible (although the observed differences between $SFR_{[O\,II]}$ and $SFR_{H\beta}$ could be a result of that, see below).

$SFR_{[O\,II]}$ and $SFR_{H\beta}$ are measured following Kewley et al. (2004) and Kennicutt (1998) (assuming the theoretical Hα/Hβ for Case B recombination), respectively, after applying the conversion from Salpeter (1955) to Chabrier (2003) IMF. For $SFR_{[O\,II]}$ we use Eq. 4 in Kewley et al. (2004), which does not take into account the dependence on the metallicity, because we were only able to measure the oxygen abundance 12+log(O/H) using high-S/N (>5) emission line ratio (e.g., R_{23}, see Zaritsky et al. 1994) for a small sample (15) of our galaxies. We do not believe that these 15 galaxies can be representative of the entire sample used for our analysis; therefore, we avoided using an average value of 12+log(O/H) from this small sample to correct $SFR_{[O\,II]}$. We find a good agreement between $SFR_{[O\,II]}$ and the SFR measured from SED fitting, with negligible bias (median ΔlogSFR=-0.001) and scatter of 0.3 dex, which is a re-

[1] Though the SFR-M_* relation from Tomczak et al. (2016) was constrained using UV+IR SFR estimates, we found that for our sample the differences between SFR_{UV+IR}, from Muzzin et al. (2013), and $SFR_{\rm SED}$ are minimal (median ΔlogSFR=-0.09 with scatter of 0.38 dex).

[2] An additional cut is included in the "SED sample" and "[O II] sample", removing 9 and 2 galaxies, respectively, because they showed low quality sSFR and/or σ_{stars} measurements (i.e., relative errors larger than one).

flection of the different timescales probed by the two tracers of star formation, as well as uncertainties in both processes. $SFR_{H\beta}$ is in less good agreement with SFR_{SED}, with median ΔlogSFR=-0.11 (scatter equal to 0.22 dex), and $SFR_{[O\,II]}$, which is in general 0.16 dex lower. As mentioned before, these differences may be due to an over correction of the underlying stellar absorption. However, at this point we are not able to draw a definite conclusion, and an investigation of these differences is beyond the scope of this work. For this reason, we decided to perform our analysis using the three tracers of star formation separately, allowing to compare the results. The value of $sSFR_{SED}$ used in the analysis presented in the next section are taken from the COSMOS2015 catalog and are computed through SED fitting, while $sSFR_{[O\,II]}$ and $sSFR_{H\beta}$ are computed as SFR/M_*, using M_* measurements from COSMOS2015.

4. SSFR - σ CORRELATION

In this section we investigate the possible correlation between stellar feedback and stellar/gas kinematics of star-forming galaxies at $0.6 < z < 1$. Kinematics can be measured using different tracers, such as stars and neutral or ionized gas. Stellar and gas kinematics generally trace each other both in simulations and observations (e.g., El-Badry et al. 2016; Cicone et al. 2016), with gas used as the preferred tracer because it is comparatively easier to detect due to the emission lines it produces. However, gas is *directly* coupled to stellar feedback, and as a consequence gas kinematics reacts to feedback on short timescales. Conversely, stars are not directly affected by feedback, but rather by the change in gravitational potential caused by feedback-driven outflows. Therefore, stellar kinematics is in principle a better tracer of the underlying potential, while gas kinematics can be affected by local turbulence caused by star formation. The LEGA-C survey provides high quality measurements of both stellar and gas kinematics; therefore, we performed our analysis using both, allowing us to investigate if differences exist. This is the first time that this investigation has been done for both stellar and gas kinematics at intermediate redshift.

We divided our SED, [O II] and Hβ samples (see Section 2) in three bins of stellar mass (M_{low}, M_{med} and M_{high}) with median values of $10^{10.0}$, $10^{10.5}$, $10^{10.9}$ $M_\odot$, and studied the correlation between the gas and stellar velocity dispersions (σ_{gas}, σ_{stars}) and sSFR in each M_* bin. The mass range in each bin (delineated by vertical lines in the right-hand panel of Figure 1) is chosen to be a compromise between having a significantly large number of galaxies and same median M_* in the three samples. We proceeded with the analysis by fitting a relation between σ and sSFR, adopting a linear least-squares approach (Cappellari et al. 2013) that accounts for the uncertainties in both parameters and incorporates the measurement of the intrinsic scatter rms_{intr} on the velocity dispersion (the best-fit parameters are reported in Table 1). The primary purpose of fitting a relation is to allow us to quantify the scatter around the possible correlation between σ and sSFR. However, the best-fit relation does not provide a good estimation of the strength and significance of the correlation. For this reason, we predominantly base our analysis on the non-parametric Spearman rank correlation parameter ρ, as well as the two-sided p-value, which provides the probability of the null hypothesis in which the data are uncorrelated. We reject the null hypothesis for p-value<0.05. The results of this analysis are presented in Figure 2.

We find that in general there exists a significant correlation between σ_{star} (and σ_{gas}) and sSFR for the galaxies in the M_{low} bin of all the three samples, except for $\sigma_{gas} - sSFR_{SED}$, where the correlation is not significant (p-value=0.16). This correlation appears to be strongest and most significant for $\sigma_{star} - sSFR_{[O\,II]}$, $\rho = 0.34$ at $>4\sigma$ significance (p-value$= 2.4e-05$), and somewhat less strong, $\rho \sim 0.15 - 0.26$, but still significant ($\gtrsim 2.5\sigma$) for the other samples. Moreover, this correlation is robust against jackknife re-sampling, the removal of galaxies with very high sSFR ($sSFR > 10^{-8}\,yr^{-1}$), and the removal of galaxies with very low stellar mass ($M_* < 10^{9.4}\,M_\odot$). We do not find any significant correlations in the higher mass bins (M_{med} and M_{high}) for all the samples, as shown by the Spearman rank correlation parameter ρ and the p-value reported in the bottom-left corner of the plots in Figure 2. The lack of significant correlation is also clear from the best-fit slopes reported

Table 1. Best-fit parameters of the σ–sSFR relations

		a	**b**	$\mathbf{x_0}$	$\mathbf{rms_{intr}}$
σ_{stars}	M_{low}	2.042(±0.012)	0.128(±0.044)	-8.78	0.144(±0.011)
vs	M_{med}	2.091(±0.009)	-0.006(±0.025)	-9.02	0.110(±0.008)
$sSFR_{SED}$	M_{high}	2.190(±0.009)	-0.041(±0.022)	-9.47	0.097(±0.008)
σ_{gas}	M_{low}	1.893(±0.013)	0.119(±0.046)	-8.78	0.187(±0.010)
vs	M_{med}	2.041(±0.011)	-0.058(±0.033)	-9.02	0.160(±0.009)
$sSFR_{SED}$	M_{high}	2.163(±0.013)	0.003(±0.033)	-9.45	0.158(±0.011)
σ_{stars}	M_{low}	2.018(±0.015)	0.116(±0.046)	-8.64	0.136(±0.014)
vs	M_{med}	2.081(±0.013)	0.028(±0.036)	-8.88	0.125(±0.011)
$sSFR_{H\beta}$	M_{high}	2.195(±0.016)	0.008(±0.035)	-9.52	0.103(±0.014)
σ_{gas}	M_{low}	1.916(±0.017)	0.179(±0.051)	-8.64	0.179(±0.014)
vs	M_{med}	2.032(±0.017)	0.002(±0.045)	-8.88	0.169(±0.013)
$sSFR_{H\beta}$	M_{high}	2.155(±0.018)	0.037(±0.039)	-9.52	0.120(±0.015)
σ_{stars}	M_{low}	2.056(±0.013)	0.191(±0.036)	-8.63	0.120(±0.014)
vs	M_{med}	2.109(±0.010)	0.074(±0.024)	-8.98	0.100(±0.010)
$sSFR_{[O\,II]}$	M_{high}	2.204(±0.011)	-0.025(±0.024)	-9.41	0.099(±0.010)
σ_{gas}	M_{low}	1.904(±0.015)	0.130(±0.042)	-8.63	0.180(±0.012)
vs	M_{med}	2.056(±0.014)	0.023(±0.033)	-8.98	0.155(±0.011)
$sSFR_{[O\,II]}$	M_{high}	2.199(±0.015)	0.013(±0.034)	-9.41	0.157(±0.012)

The relations are expressed as $y = a + b(x - x_0)$, where y represents logσ_{star} or logσ_{gas}, x is logsSFR and x_0 is the "pivot" value adopted to minimize the correlation between the errors on a and b. M_{low}, M_{med} and M_{high} refer to the three mass bins with median $M_* = 10^{10.0}$, $10^{10.5}$, $10^{10.9}$ $M_\odot$. rms_{intr} is the intrinsic scatter on the y variable and is expressed in dex.

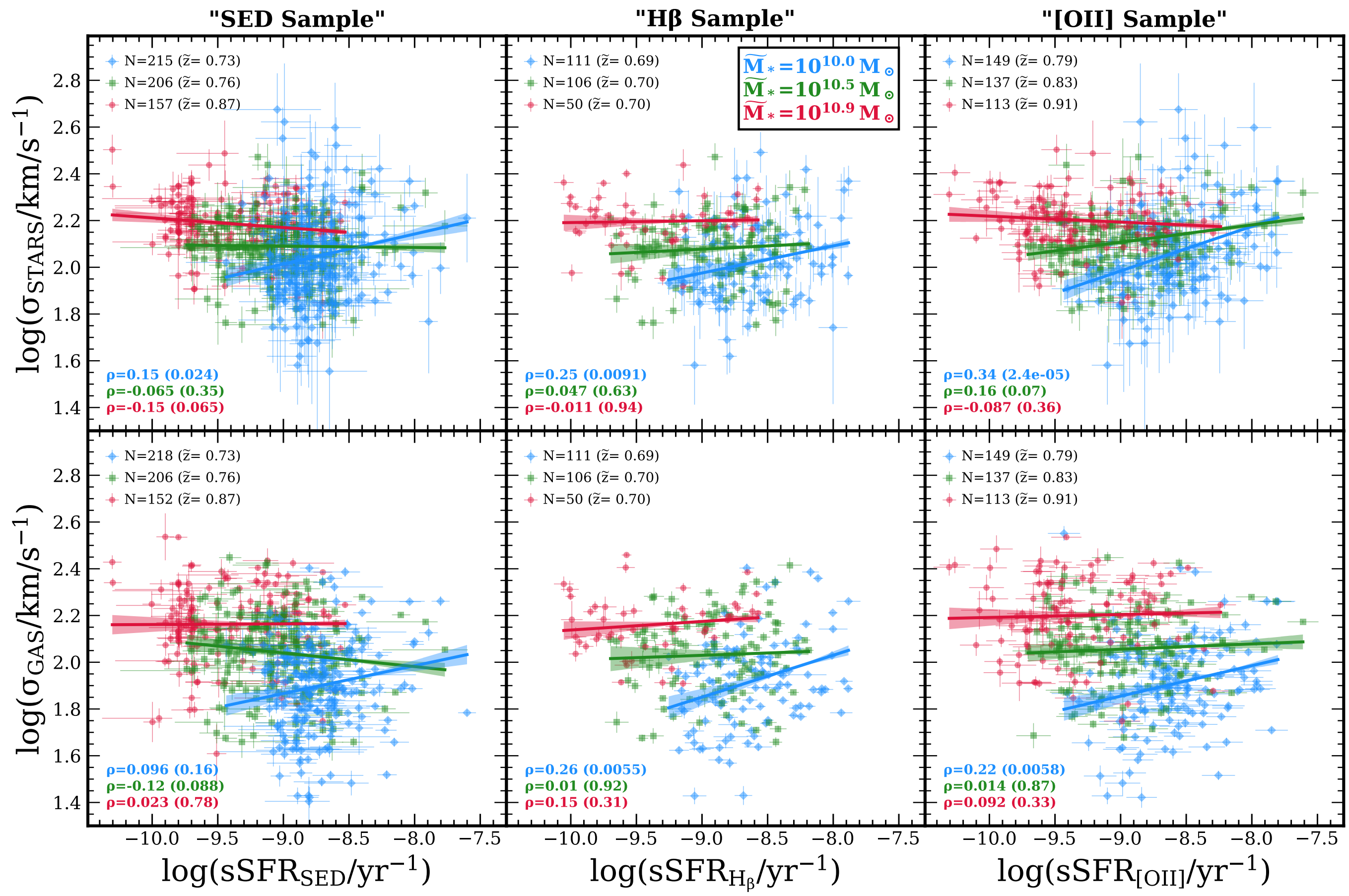

Figure 2. σ_{stars} (top row) and σ_{gas} (bottom row) as a function of the sSFR for the SED (left panels), Hβ (middle panels) and [O II] (right panels) sample (see Section 2). Blue diamonds, green squares and red circles represent galaxies with median $M_* = 10^{10.0}$, $10^{10.5}$, $10^{10.9}$ $M_\odot$, respectively. The blue, green and red solid lines with shaded areas show the best-fit relations with 1σ uncertainties for the galaxies in each mass bin (see Section 4). The number of galaxies in each mass bin and the median redshift is shown in the top-left corner of each panel. The Spearman rank correlation coefficient in each mass bin is reported in the bottom-left corner of each panel, along with the corresponding two-sided p-value given in parenthesis (see Section 4).

in Table 1, which have values close to zero for galaxies in $M_{\rm med}$ and $M_{\rm high}$, and generally large uncertainties.

We are aware of the existence of a known large scale structure (LSS) at $z \approx 0.72 - 0.76$ (Scoville et al. 2007; Betti et al. 2019) in the COSMOS field. To verify that our results are not affected by this overdensity, we repeated the analysis removing the galaxies within the LSS redshift range. We found that our main results remain unchanged, and we still observe a significant correlation between σ and sSFR for the galaxies in $M_{\rm low}$.

4.1. *Scatter Around the Relations*

We found that the intrinsic scatter rms_{intr} around the relations in Figure 2 is in general larger when using σ_{gas} than σ_{star} (see Table 1). As mentioned before, stellar and gas kinematics generally trace each other. However, while stellar kinematics is affected by changes in gravitational potential caused by stellar feedback, gas kinematics is directly affected by stellar feedback. Recent studies (e.g., Hung et al. 2019) showed that local gas turbulence, which can also be caused by stellar feedback, correlates with SFR in both observations and simulations, although with a fairly large scatter that is likely caused by a temporal delay in the time evolution of these two quantities. Therefore, while the σ_{gas}–sSFR correlation globally provides a connection between the gravitational potential and stellar feedback, in the same way as the σ_{star}–sSFR correlation does, it could also reflect stochastic short timescale gas turbulence which may increase the measured scatter.

We investigated the origin of the scatter around the relations by studying its dependence on other galaxy parameters. To this end, we focus only on the galaxies in the lowest mass bin $M_{\rm low}$ (which show significant correlations) and we computed the scatter as the deviation d_w in σ_{star} or σ_{gas} of each galaxy from the corresponding relation, weighted by the uncertainties on their measurements. We note that the errors on σ_{star} and σ_{gas} (provided with the LEGA-C DR2, see Section 2.1) constitute the formal uncertainties from the pPXF fitting.

We placed the measured d_ws into bins of sSFR, M_*, galaxy inclination and misalignment (ΔPA) between the galaxy position angle (PA) and slit PA[3], and investigate possible trends with these parameters.

We find that in general $d_w(\sigma_{star})$ shows no trend with sSFR, but increases with M_* by a factor of $\sim$2 within the M_{low} bin. The observed trend with M_*, implies that even within the lowest stellar mass bin, the lower mass galaxies are those which better follow the σ_{star}–sSFR relation likely due to their shallower gravitational potential that is more easily perturbed by stellar feedback. Conversely, we find that $d_w(\sigma_{gas})$ shows an increase with sSFR by a factor of $\sim$1.5, but no trend with M_*. The trend of $d_w(\sigma_{gas})$ with sSFR could be a sign of an increase of gas turbulence with increasing SFR. For the stellar masses considered here, the average sSFR is invariant with respect to M_*; therefore, $d_w(\sigma_{gas})$ is highly affected by sSFR irrespective of M_* within this mass bin, likely causing obscuration of any possible trend of $d_w(\sigma_{gas})$ with M_*. We also find that both $d_w(\sigma_{star})$ and $d_w(\sigma_{gas})$ do not show any trend with ΔPA; however, they increase as galaxy inclination decreases (i.e., towards more face-on galaxies). The trend with inclination can be interpreted as a consequence of the fact that for small inclinations the integrated velocity along the line of sight is more affected by the galaxy inclination, and it is therefore more uncertain. All these trends (or lack of) are observed in all three samples.

We note that this analysis of the scatter around the σ–sSFR relations is based on the assumption that the estimations of the uncertainties on σ_{star} and σ_{gas} are correct. Moreover, the errors on σ_{star} are generally $\sim$2 times higher that the errors on σ_{gas}. If these uncertainties are wrong on absolute scale between σ_{star} and σ_{gas}, this would introduce an artificial inflation of the scatter around the σ_{gas}–sSFR relations. However, as long as the uncertainties are measured relatively correctly the trends should be unaffected. An investigation on the impact of the error measurements on the scatter goes beyond the scope of this Letter. We refer to future works for a more detailed characterization of the LEGA-C velocity dispersion error budget.

4.2. *Evolution with redshift*

As we can see from Figure 1 (left panel), the redshift distributions of the three samples show some differences (which are shown also in Figure 2). While the SED and [O II] samples are detected at every redshift between $z = 0.6$ and $z = 1.0$, the SED sample appears to be dominated by galaxies at $z < 0.8$ and the [O II] sample has a slightly stronger contribution from galaxies at $z > 0.8$. Moreover, Hβ emission detection drops rapidly at $z > 0.8$, and as a result the vast majority of the galaxies in the Hβ sample are at $z < 0.8$. We investigated possible effects of the redshift evolution on the results presented here, by dividing the the SED and [O II] samples in two redshift bins ($z < 0.8$ and $z > 0.8$) and repeating the above analysis. We excluded from this analysis the Hβ sample, since it has only 19 galaxies at $z > 0.8$. We find that still no significant correlation exists for the galaxies in M_{med} and M_{high} at both redshifts. Moreover, the σ_{star} – $sSFR_{[O\,II]}$ correlation for the galaxies in M_{low} is present both at $z < 0.8$ and $z > 0.8$, and the strength of this correlation increase with redshift, from $\rho = 0.32$ ($\sim 3\sigma$) at $z < 0.8$ to $\rho = 0.41$ (at $> 4\sigma$) at $z > 0.8$. The evolution of the strength of the correlation is somewhat seen also for σ_{gas} – $sSFR_{[O\,II]}$ and in the SED sample, where the correlations become too weak to be significant at $z < 0.8$, but become stronger and significant at $z > 0.8$. Indeed, we found a significant ($\gtrsim 3\sigma$) σ_{gas} – $sSFR_{SED}$ correlation at $z > 0.8$, which was not present for the overall sample. The evolution of the Spearman rank correlation parameter ρ for the galaxies in the lowest mass bin (M_{low}) is shown in Table 2.

Table 2. Redshift evolution of the Spearman ρ

	All	$\mathbf{z < 0.8}$	$\mathbf{z > 0.8}$
σ_{stars}–$sSFR_{SED}$	0.15 (0.024)	0.12 (0.17)	0.24 (0.018)
σ_{gas}–$sSFR_{SED}$	0.096 (0.16)	-0.028 (0.74)	0.22 (0.029)
σ_{stars}–$sSFR_{[O\,II]}$	0.34 (2.4e-05)	0.32 (0.0036)	0.41 (4.2e-05)
σ_{gas}–$sSFR_{[O\,II]}$	0.22 (0.0058)	0.073 (0.52)	0.32 (0.0018)

Spearman rank correlation parameter ρ, and the two-sided p-value (in parenthesis), for the galaxies in the M_{low} bin as a function of redshift. See discussion in Section 4.2.

5. DISCUSSION AND CONCLUSIONS

In this Letter we presented an investigation of the effect of stellar feedback on galaxy kinematics for a sample of star-forming galaxies at $0.6 < z < 1.0$, drawn from DR2 of the LEGA-C survey. Given the magnitude-selected nature of the survey, this sample is biased towards galaxies with high SFR at low stellar mass ($M_* \lesssim 10^{10}\,M_\odot$). We decided, therefore, to focus our analysis only on galaxies that are above the SFR-M_* relation for normal star-forming galaxies, in order to make a fair comparison across all masses (see Section 2.3).

Several works (e.g., Governato et al. 2012; Chan et al. 2015) have shown, using cosmological baryonic simulations, that feedback-driven processes are able to displace enough mass to flatten the inner distribution of dark matter in galaxies with $M_* \lesssim 10^{9.5}\,M_\odot$. Moreover, El-Badry et al. (2017) suggested that a correlation between galaxy stellar kinematics and sSFR could be used as an observational test of the role of the stellar feedback in driving potential fluctuations, and more generally in regulating the dark matter density profile of low-mass galaxies, given that stars and dark matter

[3] As a LEGA-C observing strategy, the spectra were taken by placing the slits in the VIMOS masks always in a N-S direction (see van der Wel et al. 2016). Both galaxy PA and inclination (estimated using the galaxy axis ratio) are taken from the COSMOS Zurich Structure and Morphology Catalog (Scarlata et al. 2007).

kinematically respond to potential fluctuations in similar ways (El-Badry et al. 2016). Observational hints of this correlation were shown by Cicone et al. (2016) for a large sample of isolated galaxies with $M_* \lesssim 10^{10}\,M_\odot$ in the local universe; however, at higher redshift the relationship between σ_{star} and sSFR has not yet been investigated (see Hirtenstein et al. 2019, for a study of the $\sigma_{gas}-$sSFR relation at $z \sim 2$).

We have shown here observational evidence of a positive correlation between σ_{star} and sSFR for low-mass galaxies ($M_* \sim 10^{10}\,M_\odot$) at $z \sim 0.8$, in agreement with the predictions from cosmological simulations containing baryons. This correlation holds for different tracers of the star formation, i.e, for $sSFR_{SED}$, which traces star formation on ~100 Myr timescales, and for $sSFR_{H\beta}$ or $sSFR_{[O\,II]}$, which trace star formation on ~10 Myr timescales. Theoretical prediction by El-Badry et al. (2017) showed a stronger correlation between σ_{star} and sSFR averaged over the last 100 Myr, as a consequence of ~50 Myr delay in the response of stellar kinematics to stellar feedback. Our analysis shows that the correlation is stronger for σ_{star} – $sSFR_{[O\,II]}$, e.g., for the shorter timescale star formation tracer, in agreement with Hirtenstein et al. (2019). However, the relatively large scatter around the observed correlations makes it difficult to draw a definitive conclusion. A larger sample and a better characterization of the scatter is necessary to verify this result. Our low-mass sample is slightly more massive than the galaxies predicted to feel the largest dynamical effects of stellar feedback in simulations ($M_* \lesssim 10^{9.5}\,M_\odot$). However, a precise transition stellar mass is not specified at this point in simulations; therefore, we can confirm that the mass dependence of our result is qualitatively consistent with the theoretical predictions.

We find that the positive σ_{star}–sSFR correlation becomes stronger with redshift (see Table 2). This result is in agreement with Macciò et al. (2012), who, using cosmological simulations, found that the effect of stellar feedback on galaxy gravitational potential is strongest at intermediate redshifts ($z \approx 1-2$). Moreover, at those redshifts star-forming galaxies with $M_* \sim 10^{10}\,M_\odot$ are thought not to have settled in a disk yet (e.g., Kassin et al. 2012); therefore, they have shallower potentials more easily perturbed by the stellar feedback, which is expected to be even stronger due to higher SFRs.

A significant correlation is also found between σ_{gas} and sSFR, although the scatter in this case is larger (and the correlation less strong) compared to stellar kinematics (see Table 1). We are not able to fully characterize the nature of this scatter (although some trends are observed, see Section 4.1), and further investigation is required. However, this result implies that, in absence of stellar kinematics measurements, gas kinematics is a good tracer of the effect of stellar feedback on the galaxy's gravitational potential. Finally, no significant correlation is observed between σ_{star} (and σ_{gas}) and sSFR for galaxies in the higher mass bins ($M_* \sim 10^{10.5}\,M_\odot$ and $M_* \sim 10^{10.9}\,M_\odot$). This result implies that more massive galaxies with deeper potentials are not affected by perturbations caused by stellar feedback, which is even weaker due to the decrease of gas fractions and the flattening of the SFR–M_* relation at high M_* (e.g., Genzel et al. 2015).

A larger sample of galaxies is still necessary to better constrain this relation between stellar/gas velocity dispersion and specific star formation rate for low-mass galaxies, and characterize its dependence on other galaxy parameters. The final release of the LEGA-C survey will double the currently available measurements of stellar and gas kinematics, allowing a deeper investigation of the dynamical effects of stellar feedback. Comparisons between predicted and observed correlation could become a standard technique to constrain the feedback models adopted in simulations. Therefore, this relation, like others previously established (e.g., Tully-Fisher relation, mass-size relation) may constitute an essential benchmark for verifying theoretical models of galaxy formation and evolution.

ACKNOWLEDGMENTS

Based on observations made with ESO Telescopes at the La Silla Paranal Observatory under programme ID 194-A.2005 (The LEGA-C Public Spectroscopy Survey). AW received support from NASA, through ATP grant 80NSSC18K1097 and HST grants GO-14734 and AR-15057 from STScI, the Heising-Simons Foundation, and a Hellman Fellowship.

REFERENCES

Betti, S. K., Pope, A., Scoville, N., et al. 2019, ApJ, 874, 53, doi: 10.3847/1538-4357/ab07b3

Bezanson, R., van der Wel, A., Straatman, C., et al. 2018, ApJL, 868, L36, doi: 10.3847/2041-8213/aaf16b

Calzetti, D., Armus, L., Bohlin, R. C., et al. 2000, ApJ, 533, 682, doi: 10.1086/308692

Cappellari, M. 2017, MNRAS, 466, 798, doi: 10.1093/mnras/stw3020

Cappellari, M., & Emsellem, E. 2004, PASP, 116, 138, doi: 10.1086/381875

Cappellari, M., Scott, N., Alatalo, K., et al. 2013, MNRAS, 432, 1709, doi: 10.1093/mnras/stt562

Chabrier, G. 2003, The Astrophysical Journal, 586, L133, doi: 10.1086/374879

Chan, T. K., Kereš, D., Oñorbe, J., et al. 2015, MNRAS, 454, 2981, doi: 10.1093/mnras/stv2165

Cicone, C., Maiolino, R., & Marconi, A. 2016, A&A, 588, A41, doi: 10.1051/0004-6361/201424514

El-Badry, K., Wetzel, A., Geha, M., et al. 2016, ApJ, 820, 131, doi: 10.3847/0004-637X/820/2/131

El-Badry, K., Wetzel, A. R., Geha, M., et al. 2017, ApJ, 835, 193, doi: 10.3847/1538-4357/835/2/193

Elbaz, D., Leiton, R., Nagar, N., et al. 2018, A&A, 616, A110, doi: 10.1051/0004-6361/201732370

Genzel, R., Tacconi, L. J., Lutz, D., et al. 2015, ApJ, 800, 20, doi: 10.1088/0004-637X/800/1/20

Governato, F., Zolotov, A., Pontzen, A., et al. 2012, MNRAS, 422, 1231, doi: 10.1111/j.1365-2966.2012.20696.x

Hirtenstein, J., Jones, T., Wang, X., et al. 2019, ApJ, 880, 54, doi: 10.3847/1538-4357/ab113e

Hopkins, P. F., Kereš, D., Oñorbe, J., et al. 2014, MNRAS, 445, 581, doi: 10.1093/mnras/stu1738

Hung, C.-L., Hayward, C. C., Yuan, T., et al. 2019, MNRAS, 482, 5125, doi: 10.1093/mnras/sty2970

Kassin, S. A., Weiner, B. J., Faber, S. M., et al. 2012, ApJ, 758, 106, doi: 10.1088/0004-637X/758/2/106

Kennicutt, Robert C., J. 1998, ARA&A, 36, 189, doi: 10.1146/annurev.astro.36.1.189

Kewley, L. J., Geller, M. J., & Jansen, R. A. 2004, AJ, 127, 2002, doi: 10.1086/382723

Komatsu, E., Smith, K. M., Dunkley, J., et al. 2011, ApJS, 192, 18, doi: 10.1088/0067-0049/192/2/18

Laigle, C., McCracken, H. J., Ilbert, O., et al. 2016, ApJS, 224, 24, doi: 10.3847/0067-0049/224/2/24

Le Fèvre, O., Saisse, M., Mancini, D., et al. 2003, Proc. SPIE, 4841, 1670, doi: 10.1117/12.460959

Macciò, A. V., Stinson, G., Brook, C. B., et al. 2012, ApJL, 744, L9, doi: 10.1088/2041-8205/744/1/L9

Madau, P., & Dickinson, M. 2014, ARA&A, 52, 415, doi: 10.1146/annurev-astro-081811-125615

Mollitor, P., Nezri, E., & Teyssier, R. 2015, MNRAS, 447, 1353, doi: 10.1093/mnras/stu2466

Moustakas, J., Kennicutt, Robert C., J., & Tremonti, C. A. 2006, ApJ, 642, 775, doi: 10.1086/500964

Muzzin, A., Marchesini, D., Stefanon, M., et al. 2013, ApJS, 206, 8, doi: 10.1088/0067-0049/206/1/8

Navarro, J. F., Eke, V. R., & Frenk, C. S. 1996, MNRAS, 283, L72, doi: 10.1093/mnras/283.3.L72

Navarro, J. F., Frenk, C. S., & White, S. D. M. 1997, ApJ, 490, 493, doi: 10.1086/304888

Oh, S.-H., de Blok, W. J. G., Brinks, E., Walter, F., & Kennicutt, Robert C., J. 2011, AJ, 141, 193, doi: 10.1088/0004-6256/141/6/193

Osterbrock, D. E., & Ferland, G. J. 2006, Astrophysics of gaseous nebulae and active galactic nuclei

Pelliccia, D., Tresse, L., Epinat, B., et al. 2017, A&A, 599, A25, doi: 10.1051/0004-6361/201629064

Pontzen, A., & Governato, F. 2012, MNRAS, 421, 3464, doi: 10.1111/j.1365-2966.2012.20571.x

Price, S. H., Kriek, M., Brammer, G. B., et al. 2014, ApJ, 788, 86, doi: 10.1088/0004-637X/788/1/86

Read, J. I., & Gilmore, G. 2005, MNRAS, 356, 107, doi: 10.1111/j.1365-2966.2004.08424.x

Salpeter, E. E. 1955, ApJ, 121, 161, doi: 10.1086/145971

Scarlata, C., Carollo, C. M., Lilly, S., et al. 2007, ApJS, 172, 406, doi: 10.1086/516582

Schinnerer, E., Groves, B., Sargent, M. T., et al. 2016, ApJ, 833, 112, doi: 10.3847/1538-4357/833/1/112

Scoville, N., Aussel, H., Benson, A., et al. 2007, ApJS, 172, 150, doi: 10.1086/516751

Spano, M., Marcelin, M., Amram, P., et al. 2008, MNRAS, 383, 297, doi: 10.1111/j.1365-2966.2007.12545.x

Spergel, D. N., Bean, R., Doré, O., et al. 2007, ApJS, 170, 377, doi: 10.1086/513700

Stott, J. P., Swinbank, A. M., Johnson, H. L., et al. 2016, MNRAS, 457, 1888, doi: 10.1093/mnras/stw129

Straatman, C. M. S., van der Wel, A., Bezanson, R., et al. 2018, ApJS, 239, 27, doi: 10.3847/1538-4365/aae37a

Swinbank, A. M., Harrison, C. M., Trayford, J., et al. 2017, MNRAS, 467, 3140, doi: 10.1093/mnras/stx201

Tomczak, A. R., Quadri, R. F., Tran, K.-V. H., et al. 2016, ApJ, 817, 118, doi: 10.3847/0004-637X/817/2/118

van der Wel, A., Noeske, K., Bezanson, R., et al. 2016, ApJS, 223, 29, doi: 10.3847/0067-0049/223/2/29

Worthey, G., & Ottaviani, D. L. 1997, ApJS, 111, 377, doi: 10.1086/313021

Wuyts, S., Förster Schreiber, N. M., Nelson, E. J., et al. 2013, ApJ, 779, 135, doi: 10.1088/0004-637X/779/2/135

Zaritsky, D., Kennicutt, Robert C., J., & Huchra, J. P. 1994, ApJ, 420, 87, doi: 10.1086/173544